



Dilatancy, shear jamming, and a generalized jamming phase diagram of frictionless sphere packings

Journal:	<i>Soft Matter</i>
Manuscript ID	SM-ART-12-2020-002186.R1
Article Type:	Paper
Date Submitted by the Author:	28-Jan-2021
Complete List of Authors:	babu, varghese; Jawaharlal Nehru Centre for Advanced Scientific Research, Pan, Deng; Institute of Theoretical Physics Chinese Academy of Sciences, CAS Key Laboratory of Theoretical Physics Jin, Yuliang; Institute of Theoretical Physics Chinese Academy of Sciences, CAS Key Laboratory of Theoretical Physics Chakraborty, Bulbul; Brandeis University, Sastry, Srikanth; JAWAHARLAL NEHRU CENTRE FOR ADVANCED SCIENTIFIC RESEARCH, Theoretical Sciences Unit

Cite this: DOI: 00.0000/xxxxxxxxxx

Dilatancy, shear jamming, and a generalized jamming phase diagram of frictionless sphere packings[†]

Varghese Babu,^{*a} Deng Pan,^{*b} Yuliang Jin,^{b,c‡} Bulbul Chakraborty,^d and Srikanth Sastry^{a¶}

Received Date

Accepted Date

DOI: 00.0000/xxxxxxxxxx

Granular packings display the remarkable phenomenon of *dilatancy*, wherein their volume increases upon shear deformation. Conventional wisdom and previous results suggest that dilatancy, as also the related phenomenon of shear-induced jamming, requires frictional interactions. Here, we show that the existence of isotropic jamming densities ϕ_j above the minimal density (or the J-point density) ϕ_J , leads both to the emergence of shear-induced jamming and dilatancy in frictionless packings. Under constant pressure shear, the system evolves into a steady-state at sufficiently large strains, whose density only depends on the pressure and is insensitive to the initial jamming density ϕ_j . In the limit of vanishing pressure, the steady-state exhibits critical behavior at ϕ_J . While packings for different ϕ_j display equivalent scaling properties under compression, they exhibit striking differences in rheological behaviour under shear. The yield stress under constant volume shear increases discontinuously with density when $\phi_j > \phi_J$, contrary to the continuous behaviour in generic packings that jam at ϕ_J . Our results thus lead to a more coherent, generalised picture of jamming in frictionless packings, which also have important implications for how dilatancy is understood in the context of frictional granular matter.

1 Introduction

A large variety of familiar materials, made of macroscopic or mesoscopic constituent particles, may be characterized as *granular matter*. Sands, powders and grains are some examples. Given their large sizes, the individual particles (unlike atoms and molecules in a liquid) do not exhibit spontaneous – *Brownian* – motion, and are thus referred to as being *athermal*. They flow in response to externally applied small forces, but at sufficiently high densities or applied stresses, cease to flow, or *jam*^{1,2}. Density- or stress-driven jamming is of central importance in comprehending a wide variety of complex rheological properties of granular matter, and forms an essential part of a broader understanding of the transition from flowing states of matter to non-flowing or structurally arrested states, including, *e. g.*, the glass transition.

Density-driven jamming, unjamming and yielding of frictionless hard and soft particles have been investigated extensively since the proposal of the jamming phase diagram², which has, as originally proposed, a unique density (packing fraction) at ϕ_J characterizing the jamming transition at zero temperature and shear stress. Since then it has been shown that the jamming density ϕ_j is protocol-dependent and therefore not unique^{3–10} satisfying in general $\phi_j \geq \phi_J$ ¹⁰. However, critical behavior associated with jamming, for example the scaling relationship between pressure and density, remains the same, irrespective of ϕ_j ⁸.

An early proposal that shear deformation, besides density, can induce jamming¹, has recently been explored extensively in experimental and theoretical investigations, largely of frictional, but also frictionless hard and soft sphere systems^{11–24}. In shear jamming, the development of an anisotropic contact network under shear leads to the emergence of a state of finite shear stress and pressure, with their ratio peaking at a density-dependent characteristic strain^{11–14,18–20}.

The shear-strain dependent pressure was termed *Reynolds pressure* in¹², reflecting the idea that shear jamming occurs because constant volume conditions frustrate the tendency of granular materials to dilate under shear²⁵, a phenomenon widely referred to as *dilatancy*. With a similar view, impact-driven and shear-driven jamming in dense suspensions have been related to “frustrated dilatancy” effects^{26,27}. Shear jamming and dilatancy in frictional granular matter have thus been viewed as two sides of the same coin.

^a Jawaharlal Nehru Centre for Advanced Scientific Research, Jakkur Campus, Bengaluru 560064, India.

^b CAS Key Laboratory of Theoretical Physics, Institute of Theoretical Physics, Chinese Academy of Sciences, Beijing 100190, China.

^c School of Physical Sciences, University of Chinese Academy of Sciences, Beijing 100049, China

^d Martin Fisher School of Physics, Brandeis University, Waltham, MA 02454, USA

* These authors contributed equally.

‡ yuliangjin@mail.itp.ac.cn

¶ sastry@jncasr.ac.in

† Electronic Supplementary Information (ESI) available: [details of any supplementary information available should be included here]. See DOI: 10.1039/cXsm00000x/

Reynolds' dilatancy in granular materials has been extensively investigated, motivated by the relevance of the phenomena to soil mechanics^{28,29}. Many available results suggest an intimate relationship between frictional interactions and dilatancy: stress-dilatancy relations couple dilatancy and friction between particles³⁰. Recent studies indicate that friction is important for observing shear jamming and dilatancy³¹. Numerical studies^{32–34} have reported, and experiments²⁷ have also indirectly indicated, the absence of dilatancy in frictionless systems.

These observations are at variance with the simple picture suggested by Reynolds²⁵, where dilatancy arises purely from geometric exclusion effects of hard particles, which should therefore be observed also in frictionless systems. We aim here to resolve this paradox, and demonstrate conditions under which dilatancy emerges naturally in frictionless sphere assemblies. We show that such conditions depend critically on the presence of a line of jamming points at densities ϕ_j above ϕ_J . These dense jamming points can be systematically obtained by using proper jamming protocols¹⁰, and the distinction between ϕ_j and ϕ_J was shown to be robust in the limit of large system size⁸.

In motivating our study, we note that, below ϕ_J , initially unjammed frictionless sphere assemblies develop structures under shear, with average geometric contact numbers that increase with density, which can be mechanically stabilized by friction¹⁶. If the unjammed configurations are at densities above ϕ_J , shear deformations may create contact networks that satisfy the isostatic jamming condition for frictionless packings which are mechanically stable, leading to the possibility of both shear jamming and dilatancy. Thus, the absence of dilatancy³³ and shear jamming³² in earlier studies could be due to the failure to obtain unjammed initial configurations above ϕ_J rather than to the absence of friction. Mean-field theories, which are exact in large dimensions, indeed predicted the possibility of shear jamming²⁴ and shear dilatancy³⁵ in deeply annealed glasses of thermal hard spheres, where friction is absent. However, it is not clear if these two effects can be indeed disentangled from friction in realistic systems in physical dimensions.

In this paper, we explicitly demonstrate the phenomena of shear jamming and dilatancy in two simulated frictionless granular models (see Electronic Supplementary Information (ESI) † for details) in three dimensions, and propose a concrete method for experimental verifications. Both effects emerge in systems with $\phi_j > \phi_J$, and vanish as $\phi_j \rightarrow \phi_J$, consistent with previous studies^{32,33,36}. The *steady-states* in the large strain limit are governed by a universal equation of state (EOS), while the EOS for the initially isotropically jammed states at zero strain depends on the preparation protocol. This difference results in a discontinuous jump of the yield stress at ϕ_j for $\phi_j > \phi_J$, generalizing (in the athermal case) the Liu-Nagel jamming phase diagram².

2 Models and Methods

Two independent protocols are used to create initially unjammed states that jam at different jamming densities ϕ_j (where an isostatic force network emerges) under isotropic compressions. (i) Mechanical annealing of the bi-disperse (BD) system by the application of cyclic athermal quasistatic shear (AQS) results in un-

jamming of packings in the density range above $\phi_j \simeq 0.648$, as described in³⁷. These unjammed configurations correspond to packings with jamming densities $\phi_j \in [0.648, 0.661]$. (ii) Thermal annealing of the poly-disperse (PD) system, with the help of an extremely efficient Monte Carlo algorithm which involves artificial swap dynamics³⁸, is used to generate configurations with jamming densities $\phi_j \in [0.655, 0.69]$, above $\phi_J \simeq 0.655$ (see ESI † for more details). We then apply uniform AQS (see ESI †) to the initial configurations, under both constant volume and constant pressure conditions, in order to investigate shear jamming and dilatancy. For the constant pressure shear, we isotropically compress the system initially at ϕ_j and $P = 0$ to the desired pressure before the first shear step. We clarify that the observations here under quasistatic shear do not always apply when shear rates are finite.

3 Results and discussions

We first show that an unjammed configuration at $\phi < \phi_j$, where $\phi_j > \phi_J$, can be jammed at a certain strain γ_j by uniform constant volume AQS. The onset of shear jamming is characterised consistently by a steep increase of the shear stress σ_{xz} (Fig. 1(a) and (b)), of the non-rattler contact number Z_{NR} (Fig. 1(c)), of the pressure (Fig. S1(a) and (b) and Fig. S2 of ESI †), and of the potential energy PE (Fig. S1(c) and (d)), around γ_j . We observe that Z_{NR} exceeds the isostatic value $Z_{iso} = 2D = 6$, where $D = 3$ is the spatial dimensionality, for $\gamma > \gamma_j$, indicating that the shear jammed systems are mechanically stable. The non-rattler contact number Z_{NR} jumps discontinuously at γ_j (Fig. 1(c)), associated with an abrupt increase of the potential energy PE (Fig. 1(d)). The value of γ_j , as well as the stress overshoot amplitude, depends on the distance to the isotropic jamming $\Delta\phi = \phi_j - \phi$, and the value of ϕ_j that characterizes the degree of mechanical/thermal annealing in the initial preparation procedure (Fig. 1 (b)). The data of $PE(Z_{NR})$, on the other hand, follow a universal function on the jamming side $Z_{NR} > Z_{iso}$, that is independent of the jamming strain γ_j , the model, and the jamming protocol (shear or compression), see (Fig. 1(d)). The data for $\phi_j \approx \phi_J$ in Fig. 1(b) also offers a clear visual demonstration (to be more precisely shown later) that shear jamming disappears in the limit $\phi_j \rightarrow \phi_J$.

We next show that packings with $\phi_j > \phi_J$ dilate under constant pressure AQS (see ESI † Fig. S7 for constant volume shear). For this purpose, we modify the original AQS protocol, which is based on energy minimization at constant volume, to minimize instead the enthalpy, allowing changes in the volume of the simulation box to ensure a fixed pressure (see Sec. S2 of ESI †). In this constant pressure AQS protocol, the system traverses only those potential energy minima that have the specified pressure, P . Since the pressure is finite, the system is jammed throughout this process. For both BD and PD models, during the constant pressure shear deformation the system dilates until reaching a steady-state at packing fraction ϕ_s , that depends on the pressure applied (Fig. 2). Correspondingly, the stress σ_{xz} increases initially with strain, and eventually also reaches a steady-state plateau after an overshoot (Fig. 2(b) and 2(d)). The magnitude of stress overshoot is more significant in systems with larger ϕ_j . The presence of a maximum at a characteristic value of the strain is the

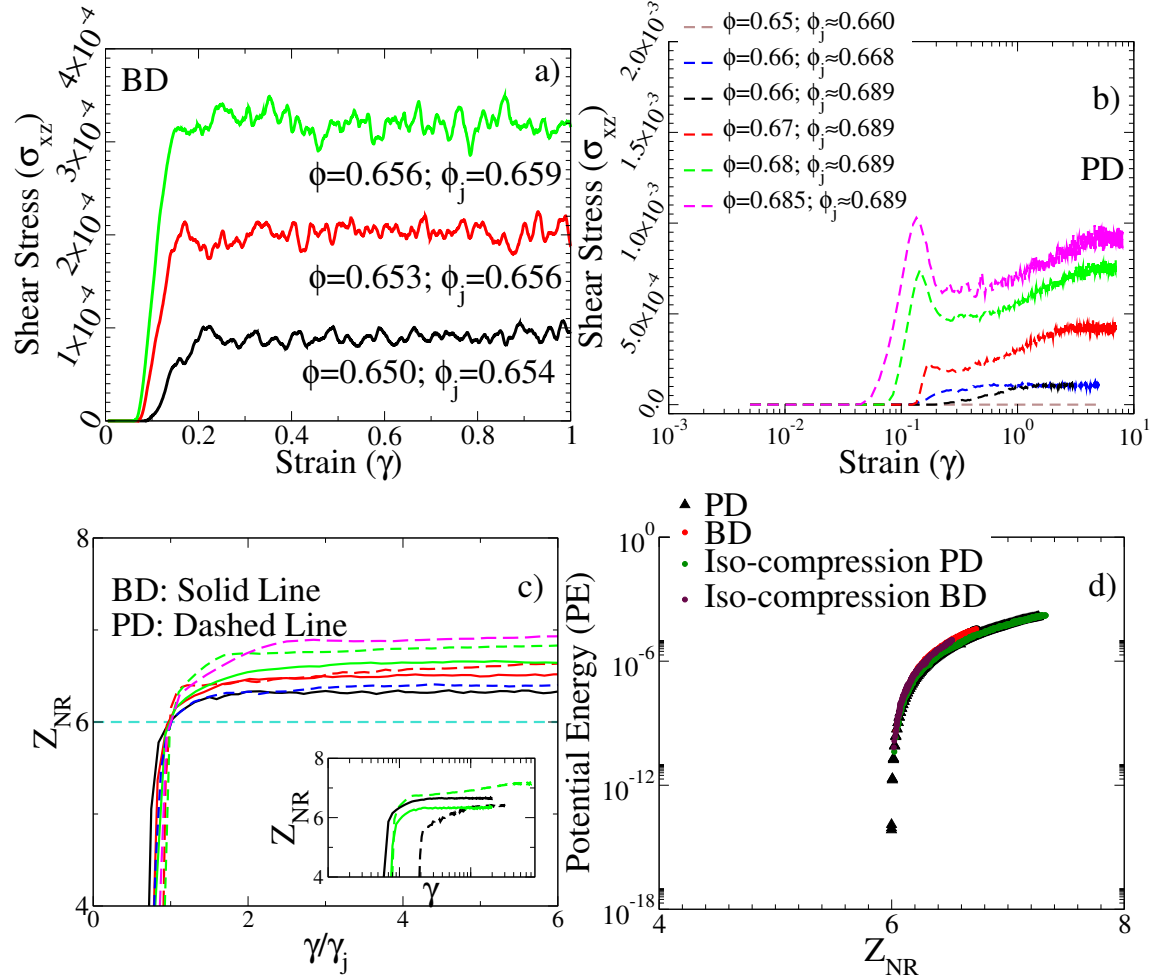


Fig. 1 Shear jamming. Shear stress σ_{xz} as a function of strain γ for (a) BD model, (b) PD model, and a few different ϕ_j and ϕ . (c) Non-rattler contact number Z_{NR} , which is calculated after removing rattlers (particles with less than $D+1$ contacts) recursively, as a function of γ/γ_j . Inset shows unscaled data, configurations at different densities jam at different strains. (d) The potential energy PE is a universal function of Z_{NR} above jamming, for both BD and PD systems, for different ϕ_j and ϕ (and therefore different γ_j), and for both compression and shear jamming. The data are averaged over 20 and 64 independent samples in BD and PD systems respectively.

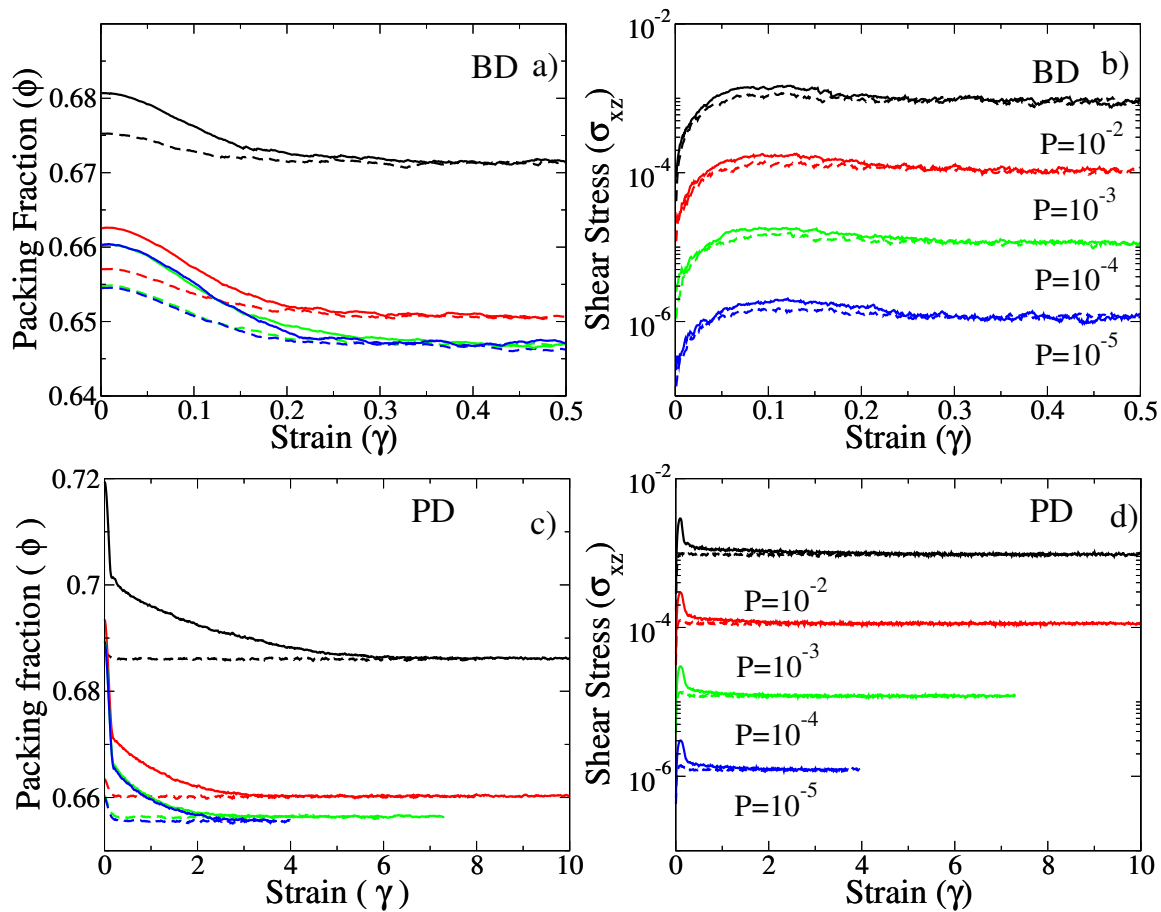


Fig. 2 Dilatancy. The evolution of (a) packing fraction ϕ and (b) shear stress σ_{xz} as functions of strain γ under constant pressure AQS in the BD model, for $\phi_j = 0.654$ (dashed) and $\phi_j = 0.66$ (solid), and for a few different pressures P (indicated in (b)). (c,d) Same data in the PD model (P values indicated in (d)), for $\phi_j = 0.660$ (dashed) and $\phi_j = 0.689$ (solid). The data are averaged over 10 and 64 independent samples in BD and PD systems respectively.

constant pressure analog of the maximum in stress anisotropy observed in the constant volume protocol as shown in the ESI †Fig. S3 (a) and (b). The development of the maximum in the stress anisotropy, or in the macroscopic friction $\mu = \sigma_{xz}/P$, therefore, seems to be a universal feature associated with shear jamming and dilatancy, in both frictionless¹⁵ and frictional systems, under both uniform^{14,22,39,40} and cyclic shear deformations²⁰.

The degree of dilation, $\delta\phi = \phi_{init} - \phi_s$, where ϕ_{init} is the initial density, increases with ϕ_j and decreases with P , as seen from Fig. 2(a) and 2(c) and shown in Fig. S4 of ESI †. In the limit $\phi_j \rightarrow \phi_J$ and $P \rightarrow 0$, the dilation effect disappears ($\delta\phi \rightarrow 0$), which is consistent with previous results³³. The PD model shows more significant dilation, because higher ϕ_j , relative to ϕ_J , is obtained, thanks to the efficient swap algorithm. We emphasize that the dilatancy effect characterized by $\delta\phi$ is a steady-state property that is distinct from the increase of Reynolds pressure, which occurs at small strains under constant volume conditions and does not extend beyond yielding^{12,24,41}. In contrast, the steady-state behavior is reached asymptotically at large strains often after many plastic failure events.

The steady-states follow the EOSs, $P_s(\phi_s)$ and $\sigma_{xz,s}(\phi_s)$, which are independent of initial conditions (ϕ_j), as shown in Fig. 3(a) and 3(b). Extrapolating the EOSs to the limit of zero pressure and stress, we find that the steady-states converge to a *critical state* at density ϕ_c , i.e., $P_s(\phi_s \rightarrow \phi_c) \rightarrow 0$ and $\sigma_{xz,s}(\phi_s \rightarrow \phi_c) \rightarrow 0$, where $\phi_c \approx 0.648$ for the BD and $\phi_c \approx 0.656$ for the PD models (Fig. 3(c)). Within our numerical precision, the critical-state density ϕ_c coincides with the J-point density ϕ_J in large systems (see Fig. S5 in ESI †for finite-size analysis), $\phi_c \simeq \phi_J$, which confirms the absence of dilatancy in the limit $\phi_j \rightarrow \phi_J$. Our observation is qualitatively consistent with the mean-field theory⁴², which suggests that shear jamming (and therefore dilatancy as well) diminishes with poor annealing.

Despite the fact that the steady-state stress is anisotropic, $P_s(\phi_s)$ agrees well with the isotropic EOS, $P_{iso}(\phi)$, obtained by an isotropic compression from ϕ_J (Fig. 3(a)). The critical scaling of P_s also obeys a linear relationship, $P_s(\phi_s) \sim \phi_s - \phi_c$, as in the isotropic jamming case, where $P_{iso} \sim \phi - \phi_J$ ⁴³. Fig. 3(a) further shows that, up to a scale factor, the EOSs for pressure collapse onto the same master curve, that is not only independent of the initial condition (ϕ_j), but also the polydispersity (BD or PD model), and the jamming protocol (constant volume shear, constant pressure shear, or isotropic compression). The stress EOSs $\sigma_{xz,s}(\phi_s)$ of steady-states (Fig.3(b)) for different shear protocols collapse on to a master curve, but unlike pressure, we cannot compare with the isotropic compression case, where the shear stress is always zero. Fig. 3 (c) shows the steady-state packing fraction ϕ_s vs. pressure, indicating more clearly the approach to the asymptotic density ϕ_c as pressure goes to zero, independently of protocol, but the value of ϕ_c is different for the two studied systems. Figure 3 (d) shows that, the macroscopic friction of steady states $\mu_s = \sigma_{xz,s}/P_s$ is non-zero, and slowly decreases with pressure as $\mu_s = \mu_0 - cP_s^\beta$ ⁴⁴, where $\mu_0 = 0.113, \beta = 0.453$ for the BD model, and $\mu_0 = 0.122, \beta = 0.458$ for the PD model. The exponent β is model-independent within the numerical er-

ror and close to (and not distinguishable within the precision of our data from) the value of 0.5 reported in⁴⁴. The values of μ_0 are also close to the previously reported data $\mu_0 \simeq 0.1$ for mono-disperse spheres with Hertzian interactions³³. This scaling of μ_s suggests that, near the critical-state ($\phi_s \rightarrow \phi_c$), the stress is proportional to the pressure, $\sigma_{xz,s} \sim \mu_0 P_s$, and the stress EOS is linear, $\sigma_{xz,s}(\phi_s) \sim \phi_s - \phi_c$, as confirmed in ESI †Fig. S9 (b). Further details of steady-states may be found in the ESI †, Figs. S8 and S9.

To summarize the above described behaviors on shear jamming and dilatancy, we propose a generalized zero-temperature jamming phase diagram. The original jamming phase diagram, introduced by Liu and Nagel², conjectures that, in the athermal limit, the jammed states at ϕ_J should be extremely fragile under shear – the yield stress vanishes at ϕ_J continuously from above jamming, $\sigma_Y(\phi_J) = 0$, suggesting that infinitesimal shear stress is required to yield (unjam) a packing at ϕ_J . While this picture is well supported by previous numerical studies where $\phi_j \approx \phi_J$ ^{33,43,45}, here we show explicitly a remarkable discontinuity of the yield stress σ_Y (as well as the yield pressure P_Y) at the jamming density ϕ_j , when $\phi_j > \phi_J$ (see Fig. 4 for the PD system and ESI †Fig. S10 for the BD system). This discontinuous nature is independent of the definition of σ_Y (here we define $\sigma_Y = \sigma_s$, see ESI †Fig. S11 for other definitions).

On the contrary, the pressure P_{iso} under isotropic compression vanishes continuously at ϕ_j (Fig. 4(a)), which is independent of ϕ_j , as shown previously⁸. It demonstrates the reason why under constant pressure shear, the volume expands from the initial isotropic states to the final steady-states (Fig. 2), and the unjammed states below ϕ_j jam under constant volume shear, as shown in Fig. 1. Interestingly, the yield stress σ_Y of shear jammed systems at a constant density ϕ below ϕ_j is a continuation of that of isotropically jammed ones. This observation is consistent with the universality of the EOSs as shown in Fig. 3. The stress jump $\sigma_Y(\phi_j)$ at the isotropic jamming transition point ϕ_j vanishes as $\phi_j \rightarrow \phi_J$, as does the regime of frictionless shear jamming.

4 Conclusions

We conclude by firstly comparing the dilatancy effect between amorphous and crystal/polycrystal assemblies. In the seminal paper²⁵ where the concept of dilatancy was introduced for the first time, Reynolds proposed a pure geometric mechanism based on the idea that one type of lattice packing (e.g., a tetrahedral arrangement) could expand its volume under shear by transforming into another type of lattice packing (e.g., a cubic arrangement). Here we recover the same geometric mechanism for amorphous packings, which has been missed in previous studies^{33,34}. Like lattices, the amorphous ensemble also includes multiple states with different packing densities, although jammed packings at $\phi_j = \phi_J$ are more abundant. The paths connecting these states, driven by external agitations such as shear, are accompanied by dilatancy, shear jamming, and additional rich phenomena such as avalanches, plasticity, shear softening and hardening, and yielding.

There are a couple of parallel studies^{46,47} focusing on frictionless shear jamming. Here we show that shear jamming is nec-

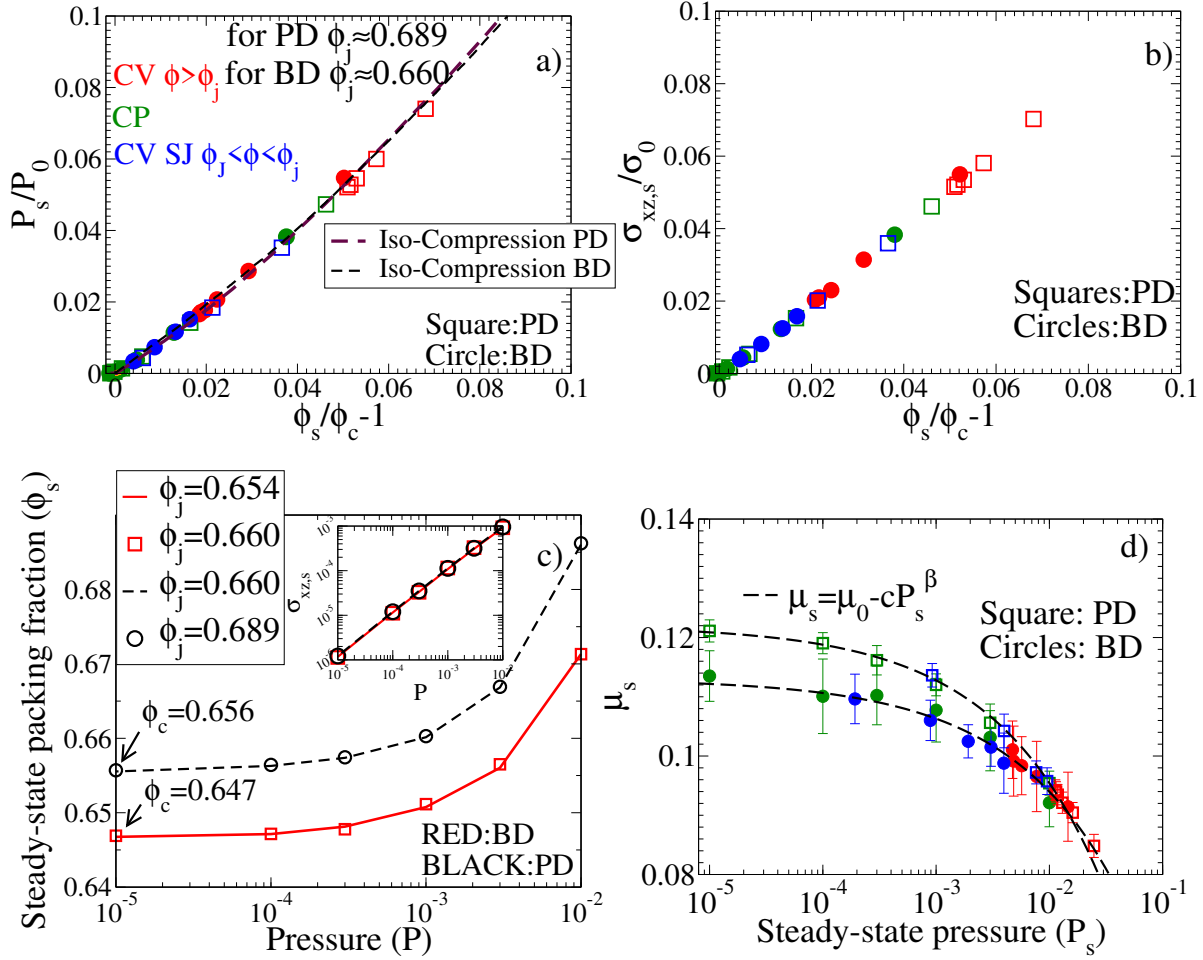


Fig. 3 Steady-state EOSs. (a) The steady-state pressure P_s is a universal function of $\phi_s/\phi_c - 1$ after rescaling. The data are obtained from constant volume shear above ϕ_j (CV, red), constant volume shear below ϕ_j where shear jamming occurs (CV SJ, blue), constant pressure shear (CP, green), and isotropic compression from ϕ_j where the rescaled P_{iso} is plotted as a function of $\phi/\phi_j - 1$. See ESI †Table S1 for the values of fitting parameters. (b) The rescaled Steady-state stress $\sigma_{xz,s}$ is a universal function of $\phi_s/\phi_c - 1$. (c) Steady-state density ϕ_s as a function of pressure P for different ϕ_j , obtained from constant pressure shear. Inset: the steady-state stress is independent of the jamming density for constant pressure shear deformation. (d) Macroscopic friction μ_s of steady-states as a function of pressure P_s .

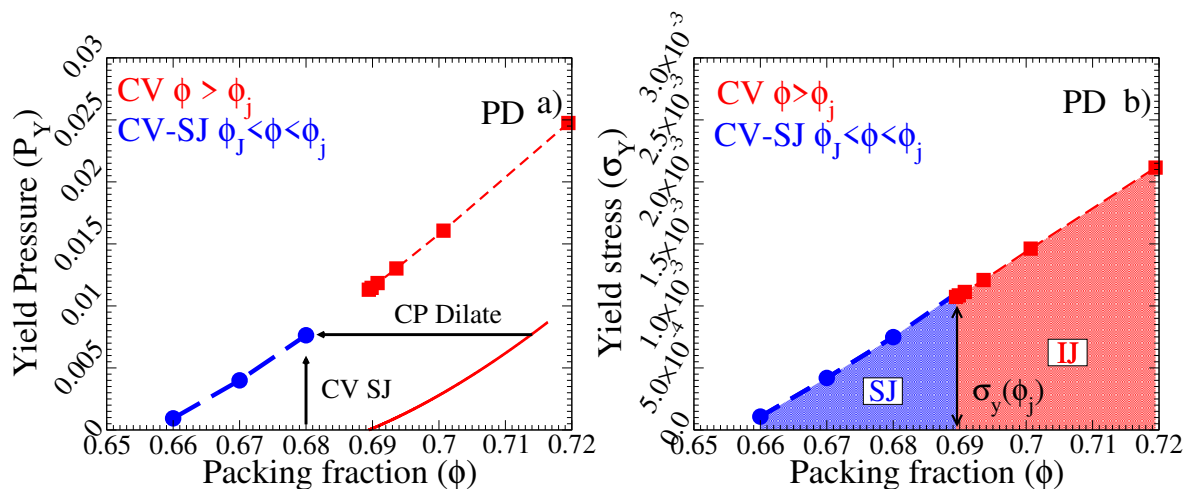


Fig. 4 Generalized zero-temperature jamming phase diagram. (a) Yield pressure P_Y (where $P_Y = P_s$) and (b) yield stress σ_Y (where $\sigma_Y = \sigma_s$) as functions of volume fraction ϕ , obtained from constant volume shear of PD systems above $\phi_j = 0.689$ (red points) and below (blue points). Above ϕ_j , the system is initially jammed by the isotropic compression (IJ), and remains jammed under shear as long as $\sigma_{xz} < \sigma_Y$, while below ϕ_j , the initially unjammed system is shear jammed (SJ) at γ_j (Fig. 1), and becomes unjammed again (yields) once σ_{xz} reaches σ_Y . The isotropic compression EOS $P_{iso}(\phi)$ is also plotted (red line). The same data are shown in Fig. 3(a) and (b) in rescaled plots.

essarily associated to another interesting phenomenon, shear dilatancy, in frictionless granular systems. We further reveal the universality of the EOSs of dilated systems (steady-states at large strains) and those of isotropic jamming (initial states at the zero strain). The evolution from the initial states to the steady-states is highly non-trivial, for which the Liu-Nagel jamming diagram has to be generalized.

Although generic protocols lead to jammed systems with $\phi_j \approx \phi_J$, where friction is necessary for dilatancy^{27,48}, here we propose a novel approach based on cyclic shear, which can be reproduced in experiments to generate packings with $\phi_j > \phi_J$ (see ESI †Sec. S10 for a concrete proposal). Our research therefore opens the way for experimental studies on exploring the complex phase space of jamming.

Conflicts of interest

There are no conflicts to declare.

Acknowledgements

We warmly thank K. Miyazaki, T. Kawasaki, and M. Otsuki for discussions. Y.J. acknowledges funding from Project 11974361, Project 11935002, and Project 11947302 supported by NSFC, from Key Research Program of Frontier Sciences, CAS, Grant NO. ZDBS-LY-7017, and from the CAS Pioneer Hundred Talents Program. BC acknowledges support from NSF-CBET-1916877, BSF-2016188, and a Simons Fellowship in Theoretical Physics. SS acknowledges support through the J. C. Bose Fellowship, SERB, DST, India. BC and SS acknowledge the support of the Indo-US Virtual Networked Joint Center project titled “Emergence and Re-modeling of force chains in soft and Biological Matter No. IUSSTF/JC-026/2016.

Notes and references

- 1 M. E. Cates, J. P. Wittmer, J.-P. Bouchaud and P. Claudin, *Phys. Rev. Lett.*, 1998, **81**, 1841–1844.
- 2 A. J. Liu and S. R. Nagel, *Nature*, 1998, **396**, 21.
- 3 R. J. Speedy, *The Journal of chemical physics*, 1994, **100**, 6684–6691.
- 4 R. J. Speedy and P. G. Debenedetti, *Molecular Physics*, 1996, **88**, 1293–1316.
- 5 R. J. Speedy, *Journal of Physics: Condensed Matter*, 1998, **10**, 4185.
- 6 F. Krzakala and J. Kurchan, *Physical Review E*, 2007, **76**, 021122.
- 7 R. Mari, F. Krzakala and J. Kurchan, *Physical review letters*, 2009, **103**, 025701.
- 8 P. Chaudhuri, L. Berthier and S. Sastry, *Physical review letters*, 2010, **104**, 165701.
- 9 G. Parisi and F. Zamponi, *Reviews of Modern Physics*, 2010, **82**, 789.
- 10 M. Ozawa, T. Kuroiwa, A. Ikeda and K. Miyazaki, *Physical review letters*, 2012, **109**, 205701.
- 11 D. Bi, J. Zhang, B. Chakraborty and R. P. Behringer, *Nature*, 2011, **480**, 355.
- 12 J. Ren, J. A. Dijksman and R. P. Behringer, *Physical review letters*, 2013, **110**, 018302.
- 13 S. Sarkar, D. Bi, J. Zhang, R. P. Behringer and B. Chakraborty, *Phys. Rev. Lett.*, 2013, **111**, 068301.
- 14 S. Sarkar, D. Bi, J. Zhang, J. Ren, R. P. Behringer and B. Chakraborty, *Phys. Rev. E*, 2016, **93**, 042901.
- 15 N. Kumar and S. Luding, *Granular Matter*, 2016, **18**, 58.
- 16 H. Vinutha and S. Sastry, *Nature Physics*, 2016, **12**, 578.
- 17 H. Vinutha, K. Ramola, B. Chakraborty and S. Sastry, *Granular Matter*, 2020, **22**, 1–8.

- 18 R. Seto, A. Singh, B. Chakraborty, M. M. Denn and J. F. Morris, Granular Matter, 2019, **21**, 82.
- 19 M. Otsuki and H. Hayakawa, Phys. Rev. E, 2017, **95**, 062902.
- 20 M. Otsuki and H. Hayakawa, Physical Review E, 2020, **101**, 032905.
- 21 Y. Jin, P. Urbani, F. Zamponi and H. Yoshino, Science Advances, 2018, **4**, eaat6387.
- 22 Y. Zhao, J. Barés, H. Zheng, J. E. S. Socolar and R. P. Behringer, Phys. Rev. Lett., 2019, **123**, 158001.
- 23 Y. Jin and H. Yoshino, Nature communications, 2017, **8**, 1–8.
- 24 P. Urbani and F. Zamponi, Physical review letters, 2017, **118**, 038001.
- 25 O. Reynolds, The London, Edinburgh, and Dublin Philosophical Magazine and Journal of Science, 1885, **20**, 469–481.
- 26 E. Brown and H. M. Jaeger, J. Rheol., 2012, **56**, 875–923.
- 27 C. Clavaud, A. Bérut, B. Metzger and Y. Forterre, Proceedings of the National Academy of Sciences, 2017, **114**, 5147–5152.
- 28 N. P. Kruyt and L. Rothenburg, Journal of the Mechanics and Physics of Solids, 2016, **95**, 411–427.
- 29 K. K. Rao and P. R. Nott, An introduction to granular flow, 2008.
- 30 P. W. Rowe, Proceedings of the Royal Society of London. Series A. Mathematical and Physical Sciences, 1962, **269**, 500–527.
- 31 R. P. Behringer and B. Chakraborty, Reports on Progress in Physics, 2018, **82**, 012601.
- 32 M. Baity-Jesi, C. P. Goodrich, A. J. Liu, S. R. Nagel and J. P. Sethna, Journal of Statistical Physics, 2017, **167**, 735–748.
- 33 P.-E. Peyneau and J.-N. Roux, Physical review E, 2008, **78**, 011307.
- 34 E. Azéma, F. Radjai and J.-N. Roux, Phys. Rev. E, 2015, **91**, 010202(R).
- 35 C. Rainone, P. Urbani, H. Yoshino and F. Zamponi, Physical review letters, 2015, **114**, 015701.
- 36 T. Bertrand, R. P. Behringer, B. Chakraborty, C. S. O'Hern and M. D. Shattuck, Physical Review E, 2016, **93**, 012901.
- 37 P. Das, H. Vinutha and S. Sastry, Proceedings of the National Academy of Sciences, 2020, **117**, 10203–10209.
- 38 L. Berthier, D. Coslovich, A. Ninarello and M. Ozawa, Phys. Rev. Lett., 2016, **116**, 238002.
- 39 S. Sarkar, E. Shatoff, K. Ramola, R. Mari, J. Morris and B. Chakraborty, EPJ Web of Conferences, 2017.
- 40 R. Seto, A. Singh, B. Chakraborty, M. M. Denn and J. F. Morris, Granular Matter, 2019, **21**, 82.
- 41 B. P. Tighe, Granular Matter, 2014, **16**, 203–208.
- 42 A. Altieri and F. Zamponi, Physical Review E, 2019, **100**, 032140.
- 43 C. S. O'Hern, L. E. Silbert, A. J. Liu and S. R. Nagel, Physical Review E, 2003, **68**, 011306.
- 44 W. Zheng, S. Zhang and N. Xu, Chinese Physics B, 2018, **27**, 066102.
- 45 C. Heussinger and J.-L. Barrat, Physical review letters, 2009, **102**, 218303.
- 46 Y. Jin and H. Yoshino, arXiv preprint arXiv:2003.10814, 2020.
- 47 T. Kawasaki and K. Miyazaki, arXiv preprint arXiv:2003.10716, 2020.
- 48 A. Singh, R. Mari, M. M. Denn and J. F. Morris, J. Rheol., 2018, **62**, 457–468.